Particles I

Access the latest eBook →

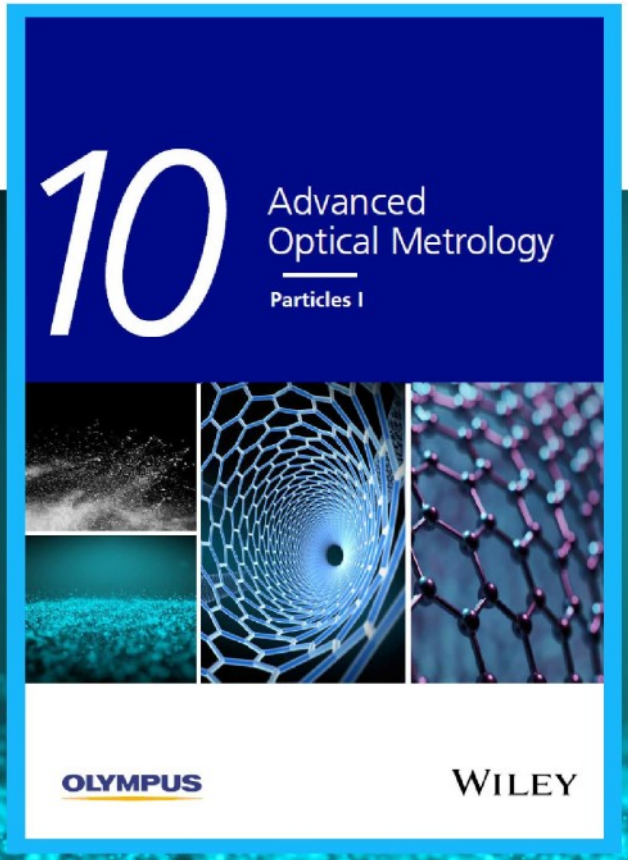

Particles: Unique Properties, Uncountable Applications

Read the latest eBook and better your knowledge with highlights from the recent studies on the design and characterization of micro- and nanoparticles for different application areas.

Access Now

This eBook is sponsored by

OLYMPUS

WILEY

ADVANCED MATERIALS
www.advmat.de

Plasmonic Nanoparticle Lattice Devices for White-Light Lasing

*Jun Guan, Ran Li, Xitlali G. Juarez, Alexander D. Sample, Yi Wang, George C. Schatz, and Teri W. Odom**

A plasmonic nanolaser architecture that can produce white-light emission is reported. A laser device is designed based on a mixed dye solution used as gain material sandwiched between two aluminum nanoparticle (NP) square lattices of different periodicities. The (±1, 0) and (±1, ±1) band-edge surface lattice resonance (SLR) modes of one NP lattice and the (±1, 0) band-edge mode of the other NP lattice function as nanocavity modes for red, blue, and green lasing respectively. From a single aluminum NP lattice, simultaneous red and blue lasing is realized from a binary dye solution, and the relative intensities of the two colors are controlled by the volume ratio of the dyes. Also, a laser device is constructed by sandwiching dye solutions between two Al NP lattices with different periodicities, which enables red–green and blue–green lasing. With a combination of three dyes as liquid gain, red, green, and blue lasing for a white-light emission profile is realized.

1. Introduction

Multicolored light sources are important for full-color displays, optical communication, and multispectral biological imaging.[1] For displays, a mixture of red, green, and blue (RGB) light is needed to produce a wide range of additive colors, where white light of different hues can result from the appropriate RGB ratios. Incoherent light sources such as lamps, cathode-ray tubes, and light emitting diodes (LEDs) cannot provide a wide color range (i.e., color gamut) due to their large RGB spectral linewidths.[2] Although recent advances in organic LEDs and quantum dot LEDs have shown a larger color gamut, only 50–70% of all colors perceptible to the human eye have been realized.[3] In contrast, lasers are coherent light sources and allow high-purity monochromic colors that can in principle extend the color range up to 78%.[4] Besides displays, emerging light-fidelity (Li-Fi) technologies use white-light sources for data transmission and illumination at the same time.[5] Because of the strong emission intensity and temporal and spatial coherence of lasers, laser-based Li-Fi devices can facilitate high-speed data rates, high modulation bandwidths, and free-space connections. Also, confocal laser scanning microscopy benefits from white-light laser sources since multiple fluorescently labeled protein probes can be simultaneously tracked to map gene expression in genetically modified tissue.[6]

To generate white-light lasing, conventional techniques either combine three individual RGB lasers or use a blue laser to excite phosphors whose yellow emission is then split into red and green light.[7] These sources require bulky optical components and precise alignment, however, which has precluded wide-spread adoption in integrated optics. Advances in laser design are needed to realize compact white laser sources. Typical semiconductors cannot support lasing colors over the full RGB wavelength range (400–700 nm) because of limited gain bandwidths (<50 nm).[8] Although emerging gain materials such as colloidal quantum dots,[9] hybrid perovskites,[10] and upconverting nanoparticles (NPs)[11] can emit RGB colors by controlling particle size, composition, or dopant ions, respectively, efficient coupling of RGB emitters to multiple cavity modes concurrently is difficult. White-light lasing has been realized in multisegment nanosheets of semiconductor alloys,[12] from dye-doped polymers integrated in layered distributed feedback structures,[13] and from dye solutions mixed with random scattering particles.[14] In the former case, fine control is required over pump-energy density in each microscale segment, while in the latter case, color manipulation is limited because controlling and changing the relative RGB intensities is not possible.

Organic dye solutions combined with plasmonic NP lattices show wavelength-tunable emission.[15,16] Because surface lattice resonances (SLRs) are hybrid modes from localized surface plasmons coupled to Bragg diffraction modes, their wavelengths can be manipulated readily by varying lattice parameters.[17] For example, changing the periodicity by mechanically stretching an elastomeric substrate allows for strain-dependent tunable laser wavelengths;[18] fabricating lattices with broken symmetry (rectangular and rhombohedral) result in polarization-dependent

J. Guan, Y. Wang, G. C. Schatz, T. W. Odom
Graduate Program in Applied Physics
Northwestern University
2145 Sheridan Road, Evanston, IL 60208, USA
E-mail: todom@northwestern.edu
J. Guan, A. D. Sample, G. C. Schatz, T. W. Odom
Department of Chemistry
Northwestern University
2145 Sheridan Road, Evanston, IL 60208, USA
R. Li, X. G. Juarez, T. W. Odom
Department of Material Science and Engineering
Northwestern University
2220 Campus Drive, Evanston, IL 60208, USA
The ORCID identification number(s) for the author(s) of this article can be found under https://doi.org/10.1002/adma.202103262.

DOI: 10.1002/adma.202103262

emission with different colors;[19,20] and leveraging high-order light-cone SLRs as cavity modes enables in-plane lasing, where different colors are emitted at different azimuthal angles.[21] One drawback of these studies is the limited tunability of lasing color (wavelength range < 60 nm) because only one type of molecular dye was used as gain. Molecular dyes, however, are soluble in a wide range of organic solvents, and different dyes can be mixed together to show RGB photoluminescence over a wide wavelength range despite reabsorption.[14,22]

Here, we show white-light lasing from a sandwiched plasmonic NP lattice device with mixed dyes. We designed a materials system that achieved red, green, and blue lasing by combining three different dye molecules as gain media with two different 2D plasmonic NP lattices as cavities. The SLR cavity modes were determined by the (±1, ±1) and (±1, 0) band-edge modes in a square a_1 = 450 nm Al NP lattice and the (±1, 0) band-edge mode in a square a_2 = 350 nm Al NP lattice. Both blue and red lasing was achieved from a single a_1 = 450 nm NP lattice with dyes whose emission overlapped with the SLR cavity modes. Green lasing was realized from a_2 = 350 nm NP lattices with a third organic dye. By combining different concentrations of two dyes in solution, we demonstrated simultaneous blue and red lasing whose relative intensities depended on the dye ratio. Sandwiching a liquid layer of two dyes between the a_1 = 450 nm NP lattice and the a_2 = 350 nm NP lattice resulted in a lasing device that emitted tunable lasing colors from a combination of red and green as well as blue and green. Incorporating three dyes into the sandwich structure and optimizing their mixing ratios resulted in simultaneous blue, green, and red lasing and white-light emission.

2. Results and Discussion

Scheme 1 illustrates the white-light laser architecture. To demonstrate red, green, and blue lasing independently, we first fabricated nanocavities with SLR modes at the desired wavelengths. Two 2D square arrays of Al NPs on fused silica were generated over cm^2-areas using solvent-assisted nanoscale embossing (SANE)[23] and PEEL[24] (**Figure 1**a). Optimized Γ-point ($k_{\|}$ = 0) SLR modes were identified by finite-difference time-domain calculations as follows: for a_1 = 450 nm, d_1 = 80 nm and height h = 60 nm; and for a_2 = 350 nm, d_2 = 70 nm, and h = 60 nm (Figure S1, Supporting Information). At the Γ point, the a_1 = 450 nm NP lattice shows (±1, ±1) and (±1, 0) SLR modes (λ = 470 and 649 nm) that are in the blue and red wavelength ranges, respectively; the a_2 = 350 nm NP lattice produces a (±1, 0) SLR mode (λ = 510 nm) in the green wavelength range (Figure 1b).

To realize lasing emission from these NP cavities, we selected C480, C500, and DCM dyes as gain materials since their photoluminescence spectrally overlap with the targeted RGB SLR modes (Figure 1a, Figure S2, Supporting Information). After dissolving the dyes in dimethyl sulfoxide (DMSO), we placed one droplet of a single dye solution on top of a Al NP lattice and covered the liquid gain with a glass slide. We optically pumped the devices using 100 fs, 400 nm laser pulses and collected the emission spectra normal to the sample surface. For each color, a sharp and intense emission peak (λ = 466, 511, 651 nm, full-width half-maximum (FWHM) ≈ 0.5 nm) emerged close to the wavelength of the SLR mode for pump intensities above a threshold of ≈0.5 mJ cm^{-2} (Figure 1b, Figure S3, Supporting Information). The lasing emission intensities were more than two orders of magnitude higher than the spontaneous emission from the dyes (Figure S2, Supporting Information).

Figure 2a shows a design to realize blue and red lasing simultaneously from the same pump source by mixing 20 × 10^{-3} M C480 and 3 × 10^{-3} M DCM in DMSO. These concentrations were selected by trial-and-error optimization since dye concentrations that were too low resulted in insufficient optical gain for lasing, and dye concentrations that were too high suppressed lasing because of non-radiative energy transfer between dye molecules. Compared to the (±1, 0) SLR band-edge mode, the (±1, ±1) mode has a lower quality factor and weaker near-field enhancement (Figure S4, Supporting Information); hence, a higher concentration of C480 dye was needed to compensate the larger cavity loss. We found that varying the volume ratios of the two dyes could manipulate the relative lasing intensities of the blue and red colors. Figure 2b shows the lasing emission spectra under different volume ratios of C480

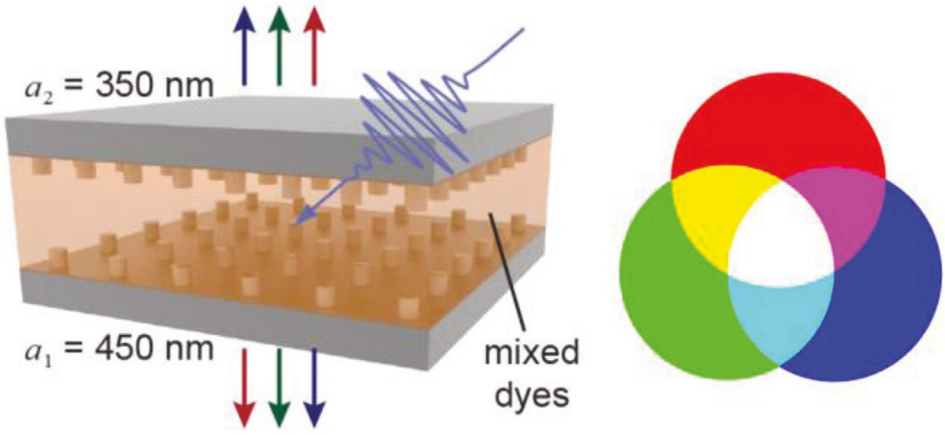

Scheme 1. White-light laser based on a sandwiched plasmonic nanoparticle lattice device.

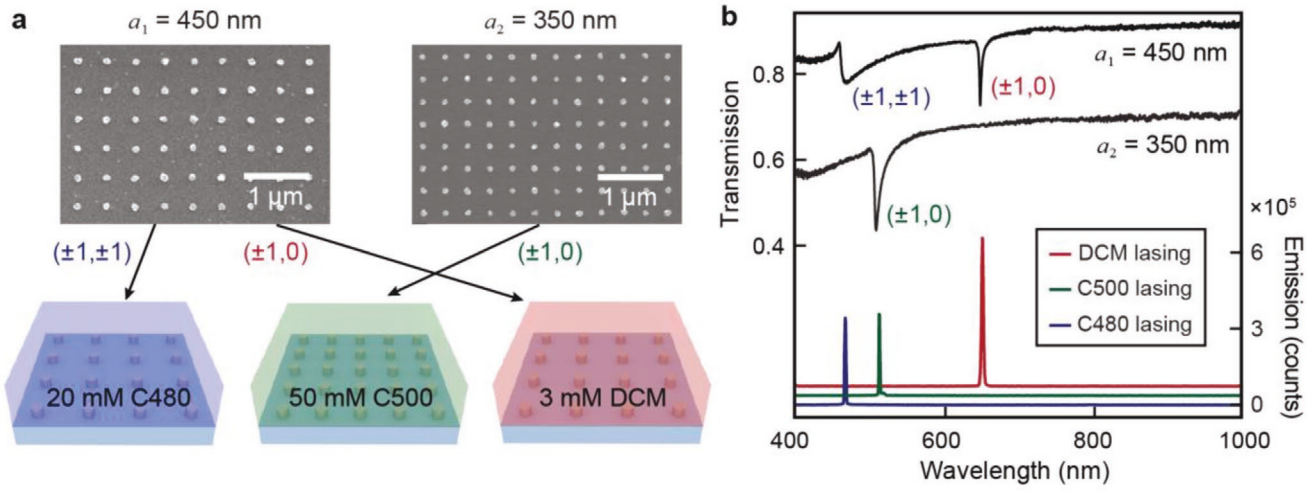

Figure 1. Blue, green, and red lasing from two plasmonic nanoparticle lattices. a) Scanning electron microscopy images of fabricated square lattices (a_1 = 450 nm and a_2 = 350 nm) of Al NPs, and schemes of three different dyes incorporated with the two lattices. b) Measured transmission spectra of the two lattices, and red, green, and blue lasing spectra. Transmission spectra of a_2 = 350 nm lattice was shifted down 0.3 for clarity. Lasing spectra of C500 and DCM are shifted up for clarity.

and DCM solutions (V_{C480}: V_{DCM}) at the same pump energy (≈1.5 mJ cm^{-2}). At a mixing ratio of 10:1, only blue lasing was observed because the low concentration of DCM did not provide sufficient gain to overcome the cavity loss at the (1,0) SLR mode; red lasing was not possible. With a volume ratio between 10:2–10:3, both blue and red lasing were supported. Increasing the volume of the DCM dye solution produced higher red lasing intensity and lower blue lasing intensity, as expected. We captured a photo of the lasing profile by placing a white piece of paper 8 cm away from the plasmonic NP lattice under high pump energy (1.8 mJ cm^{-2}); both red and blue emissions were normal to the lattice plane (Figure 2c). The lasing profiles of the red and blue emission were stretched along the (1, 0) and the (1, 1) directions, respectively, because flat SLR bands near the band edge modes can also support lasing at high pump powers; the line shapes are consistent with previously reported SLR lasing profiles.[19] The two-color lasing signals disappear in <2 s from dye reabsorption.[25]

To add a third lasing color in a single device structure, we first needed to design a NP lattice architecture that could support multiple SLR modes spanning the visible regime (**Figure 3**a). We found that a sandwich structure consisting of the a_2 = 350 nm Al NP lattice on top of the a_1 = 450 nm Al NP lattice separated by a droplet of DMSO (≈5 μL) showed sharp SLR modes independent of any in-plane translational or rotational (φ) mismatch. The extinction efficiency of this double-layer structure was a linear combination of extinction efficiencies of individual lattices because the micrometer-scale vertical

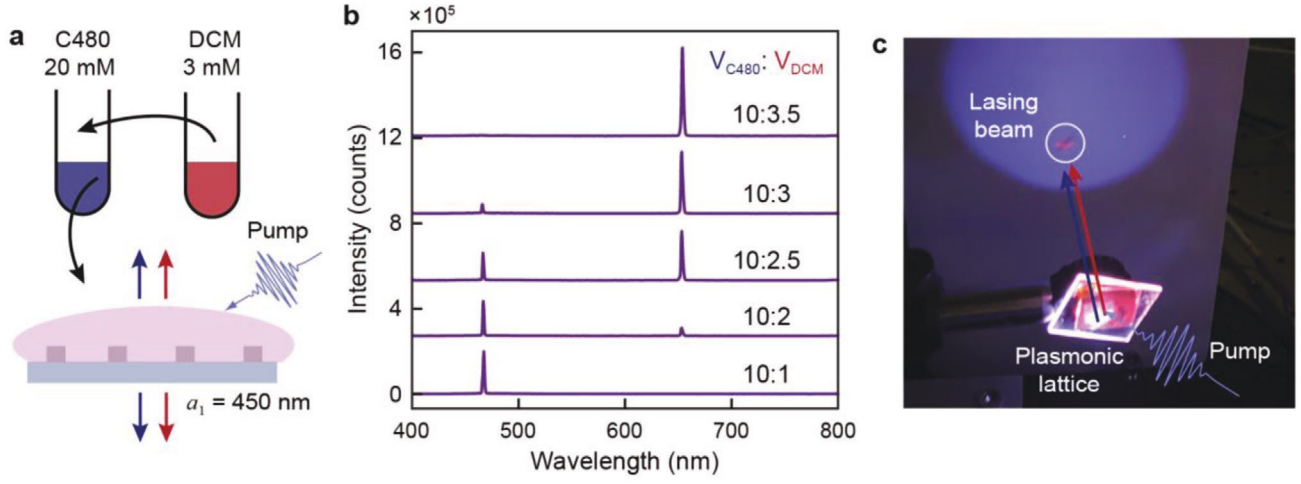

Figure 2. Control of relative lasing intensities by varying the mixing ratio of two dyes. a) Scheme of simultaneous blue and red lasing from mixed C480 and DCM dyes on an a_1 = 450 nm Al nanoparticle lattice. b) Relative lasing emission intensities can be controlled by the mixing ratio of the dyes. c) Photo of the far-field emission beam. The light purple background is the scattered pump laser beam (400 nm).

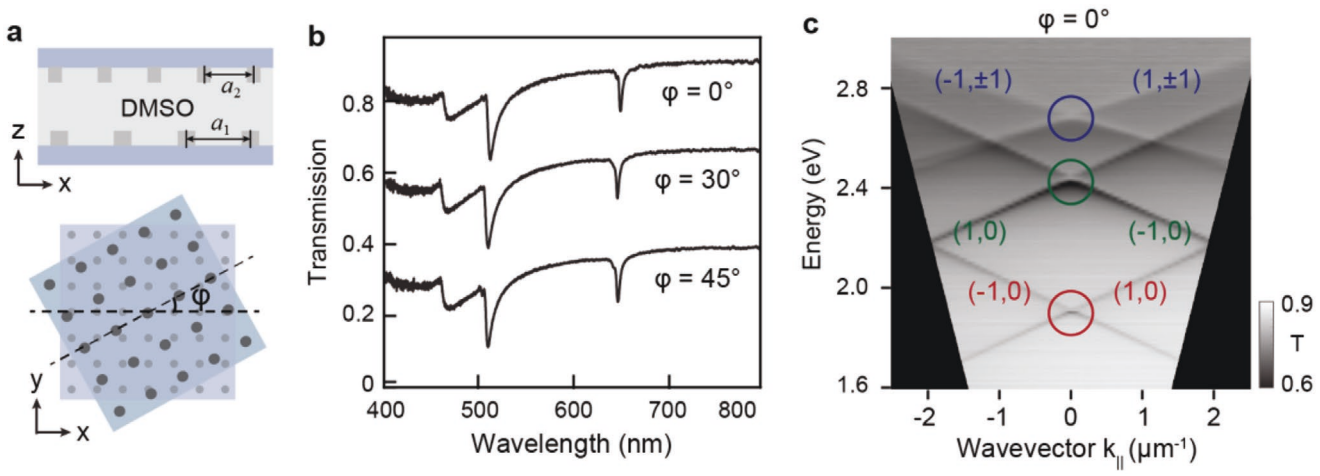

Figure 3. Three surface lattice resonance cavity modes in a sandwiched lattice structure. a) Scheme of a sandwiched plasmonic device with a relative rotation angle φ between two lattices. b) Measured transmission spectra at different angular offsets under transverse electric (TE) polarized incident light. Transmission spectra at $\varphi = 30°$ and $\varphi = 45°$ are shifted down 0.25 and 0.5 for clarity. c) Measured band structure along the Γ–X direction under TE polarized incident light.

separation between two lattices prevented interlayer NP interactions (Figure 3b). Regardless of the in-plane orientation of the lattice, the polarization direction of the incident light can be decomposed into two orthogonal directions along the x and y axes, and so each Γ-point SLR mode from a single NP lattice can be excited independent of lattice rotation. Thus, the measured SLR modes from the sandwich structure are tolerant to rotational mismatch between the two lattices, as expected. The optical band structure of the sandwiched structure shows three band-edge SLR modes with near-zero group velocities at the Γ points (Figure 3c).

We demonstrated that this sandwiched cavity structure could support two-color lasing (**Figure 4**a). Since 20×10^{-3} M C480 and 3×10^{-3} M DCM can support red and blue lasing (Figure 2), we fixed these two concentrations and determined the concentration of C500 for green lasing by considering the absorption and emission spectra of the dyes. Because the absorption of DCM partially overlaps with the emission of C500 (Figures S2 and S5, Supporting Information), a relatively high C500 concentration (50×10^{-3} M) and a high V_{C500}:V_{DCM} mixing ratio were needed to avoid quenching of C500 lasing. After mixing C500 with DCM solutions, we constructed a laser device by integrating the mixed gain material with the two Al NP lattices. The plasmonic hotspots of the different SLR cavity modes are spatially separated in the two NP lattice layers, and thus the competition between lasing modes can be minimized for more stable emission (Figure S6, Supporting Information). Under 400 nm fs pulses, simultaneous green and red lasing was achieved from the sandwiched device, whose emission intensities depended on the volume ratio of the dyes (Figure 4b). Similarly, a combination of C480 and C500 resulted in tunable colors by controlling the ratio of blue and green lasing intensities (Figure 4c).

A CIE1931 chromaticity diagram is a standard approach to characterize visible colors.[26] In theory, by mixing three elementary colors with the appropriate ratios, all colors inside

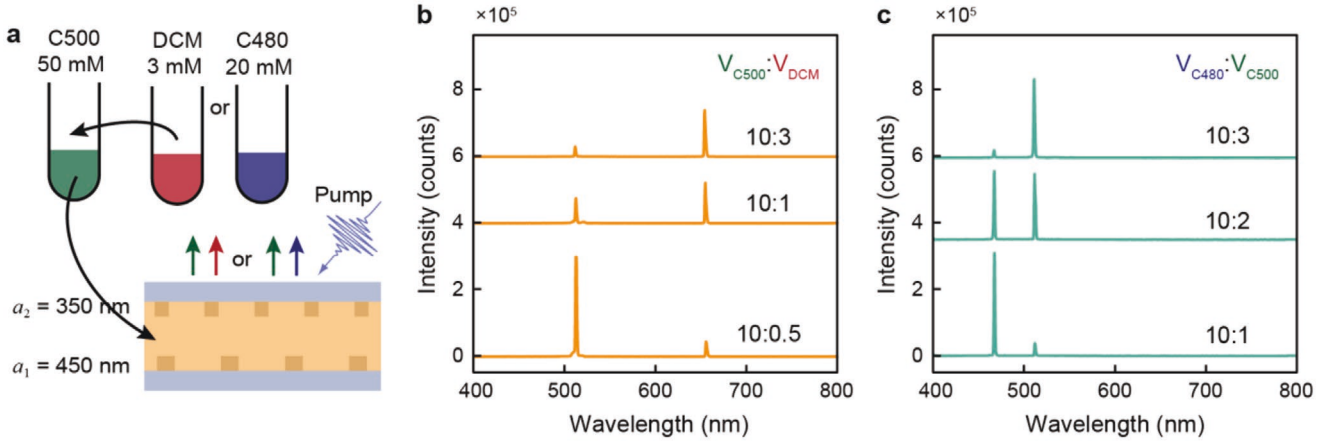

Figure 4. Tuning of lasing color in the sandwiched device. a) Scheme of a two-color laser using a sandwiched plasmonic nanoparticle device. b) Different volume ratios of C500 and DCM were used to tune the green and red lasing intensities. c) Different volume ratios of C480 and C500 resulted in controlled blue and green lasing.

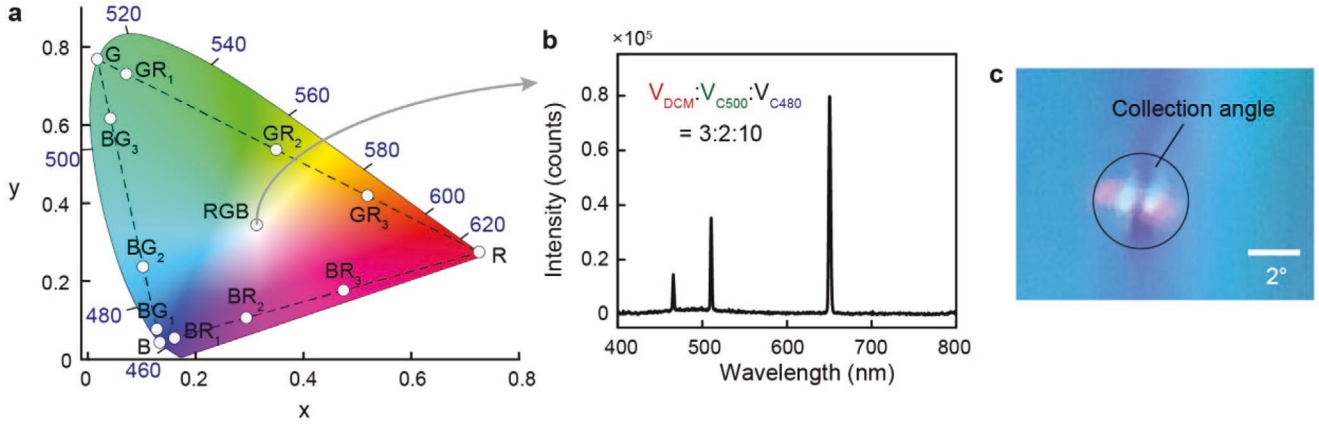

Figure 5. Realization of white-light lasing emission. a) CIE plot of lasing emission profiles. BR_1, BR_2, and BR_3 refer to the lasing spectra in Figure 2b with dye mixing ratios 10:2, 10:2.5, and 10:3. BG_1, BG_2, and BG_3 refer to the lasing spectra in Figure 4b from bottom to top, and GR_1, GR_2, and GR_3 refer to the lasing spectra in Figure 4c from bottom to top. b) Lasing emission spectra with a mixture of red, green, and blue dyes. c) Photo of the far-field emission profile. The collection angle of the CCD detector is ≈3°.

the triangle formed by the three colors can be achieved.[27] We identified the lasing colors from the measured emission spectra on a CIE plot (**Figure 5**a, Table S1, Supporting Information), where the RGB lasing colors from single dyes appear at the edge of the color space. The simultaneous blue and red lasing emission from a mixture of C480 and DCM dyes, viewed as magenta by the human eye, emerge along the line between pure blue and red colors (BR_1, BR_2, BR_3). Similarly, the simultaneous green–red lasing (GR_1, GR_2, GR_3) and green–blue lasing (BG_1, BG_2, BG_3) are shown along the other two sides of the triangle, as yellow and cyan colors. Our laser design can facilitate a large range of accessible colors because of the widely separated RGB wavelengths and the narrow lasing linewidths. To realize a white-light lasing profile, we mixed the DCM, C500, and C480 dyes with an optimized mixing volume of 3:2:10 (Figure 5b, Figure S7, Supporting Information). Since the emission of C480 dye overlaps with the absorption of C500 and DCM dyes, a larger volume of C480 solution was used to provide sufficient optical gain for the blue lasing. Figure 5c is a photo of lasing action with white-light emission at the center of the beam. The green color in the background was from the amplified spontaneous emission from the propagating SLR modes at off-normal angles.[15,28] Because the relative intensities of different lasing modes depend on pump power (Figures S6 and S8, Supporting Information), future device optimization will be needed to generate consistent colors over a wide range of pump powers.

3. Conclusion

We have realized a plasmonic white-light laser by combining a sandwiched lattice structure with a mixed dye solution. By engineering the mixing ratios of RGB dyes in multimodal plasmonic cavities, we achieved control over the relative lasing emission intensities, which enables a wide range of additive colors from a single device. Our work provides insight into how lasing colors can be manipulated in compact architectures. Looking forward, we believe that integrating plasmonic NP lattices with more efficient gain media, such as semiconducting nanocrystals and hybrid perovskites, can improve the performance of white-light nanoscale lasers with lower power consumption, higher output efficiencies, and more stable operation. Furthermore, the sandwiched plasmonic lattice architecture offers a strategy to engineer light-matter interactions over a broad wavelength range, which will be useful for display technologies, on-chip optical communications, and light-induced chemical reactions.

Supporting Information

Supporting Information is available from the Wiley Online Library or from the author.

Acknowledgements

This work was supported by the National Science Foundation (NSF) under DMR-1904385 and the Vannevar Bush Faculty Fellowship from Department of Defense (DOD) under N00014-17-1-3023. This work made use of the NUFAB facility and the EPIC facility of Northwestern University's NUANCE Center, which has received support from the SHyNE Resource (NSF ECCS-2025633), the IIN, and Northwestern's MRSEC program (NSF DMR-1720139). This research was supported in part by the Quest high performance computing facility at Northwestern University, which is jointly supported by the Office of the Provost, the Office for Research, and Northwestern University Information Technology. This work made use of the Pritzker Nanofabrication Facility part of the Pritzker School of Molecular Engineering at the University of Chicago, which receives support from SHyNE Resource (NSF ECCS-2025633), a node of the National Science Foundation's National Nanotechnology Coordinated Infrastructure.

Conflict of Interest

The authors declare no conflict of interest.

Data Availability Statement

Research data are not shared.

Keywords

lattice plasmons, multi-color lasers, plasmonic nanoparticle lattices, sandwiched devices, surface lattice resonances, white-light lasers

Received: April 28, 2021
Revised: July 14, 2021
Published online:

[1] a) J. Zhao, Y. Yan, Z. Gao, Y. Du, H. Dong, J. Yao, Y. S. Zhao, *Nat. Commun.* **2019**, *10*, 870; b) N. Granzow, *Proc. SPIE* **2019**, *11144*, 1114408. c) D. V. Patel, C. N. J. McGhee, *Clin. Exp. Ophthalmol.* **2007**, *35*, 71; d) X. Y. Liu, S. Y. Yi, X. L. Zhou, S. L. Zhang, Z. L. Fang, Z. J. Qiu, L. G. Hu, C. X. Cong, L. R. Zheng, R. Liu, P. F. Tian, *Opt. Express* **2018**, *26*, 19259; e) J. H. Choi, Y. S. No, J. P. So, J. M. Lee, K. H. Kim, M. S. Hwang, S. H. Kwon, H. G. Park, *Nat. Commun.* **2016**, *7*, 15569; f) Y. J. Lu, C. Y. Wang, J. Kim, H. Y. Chen, M. Y. Lu, Y. C. Chen, W. H. Chang, L. J. Chen, M. I. Stockman, C. K. Shih, S. Gwo, *Nano Lett.* **2014**, *14*, 4381.

[2] a) T. Z. Wu, C. W. Sher, Y. Lin, C. F. Lee, S. J. Liang, Y. J. Lu, S. W. H. Chen, W. J. Guo, H. C. Kuo, Z. Chen, *Appl. Sci.* **2018**, *8*, 1557; b) M. Schadt, *Jpn. J. Appl. Phys.* **2009**, *48*, 03B001.

[3] a) H. W. Chen, J. H. Lee, B. Y. Lin, S. Chen, S. T. Wu, *Light: Sci. Appl.* **2018**, *7*, 17168; b) J. R. Manders, L. Qian, A. Titov, J. Hyvonen, J. Tokarz-Scott, K. P. Acharya, Y. X. Yang, W. R. Cao, Y. Zheng, J. G. Xue, P. H. Holloway, *J. Soc. Inf. Disp.* **2015**, *23*, 523; c) R. D. Zhu, Z. Y. Luo, H. W. Chen, Y. J. Dong, S. T. Wu, *Opt. Express* **2015**, *23*, 23680.

[4] H. Y. Song, H. F. Li, X. Liu, *Opt. Express* **2018**, *26*, 23436.

[5] a) R. R. Chaudhuri, K. Dutta, A. Saha, *Springer Proc. Phys.* **2015**, *166*, 479; b) C. Lee, M. S. Islim, S. Videv, A. Sparks, B. Shah, P. Rudy, M. McLaurin, H. Haas, J. Raring, *Int. Soc. Opt. Photonics* **2020**, *11302*, 1130213.

[6] a) T. C. Brelje, M. W. Wessendorf, R. L. Sorenson, *Method Cell Biol.* **1993**, *38*, 97; b) S. W. Paddock, *BioTechniques* **1999**, *27*, 992.

[7] a) G. Hollemann, B. Braun, F. Dorsch, P. Hennig, P. Heist, U. Krause, U. Kutschki, H. Voelckel, *Proc. Soc. Photo-Opt. Instrum. Eng.* **2000**, *3954*, 140; b) K. V. Chellappan, E. Erden, H. Urey, *Appl. Opt.* **2010**, *49*, F79.

[8] a) R. X. Yan, D. Gargas, P. D. Yang, *Nat. Photonics* **2009**, *3*, 569; b) W. W. Chow, S. W. Koch, M. I. Sargent, *Semiconductor-Laser Physics*, Springer Science & Business Media, Berlin, Germany **2012**.

[9] D. V. Talapin, J. S. Lee, M. V. Kovalenko, E. V. Shevchenko, *Chem. Rev.* **2010**, *110*, 389.

[10] Q. Zhang, R. Su, W. N. Du, X. F. Liu, L. Y. Zhao, S. T. Ha, Q. H. Xiong, *Small Methods* **2017**, *1*, 1700163.

[11] M. Haase, H. Schafer, *Angew. Chem., Int. Ed.* **2011**, *50*, 5808.

[12] F. Fan, S. Turkdogan, Z. C. Liu, D. Shelhammer, C. Z. Ning, *Nat. Nanotechnol.* **2015**, *10*, 796.

[13] a) T. R. Zhai, Y. L. Wang, L. Chen, X. F. Wu, S. T. Li, X. P. Zhang, *Nanoscale* **2015**, *7*, 19935; b) K. Yamashita, N. Takeuchi, K. Oe, H. Yanagi, *Opt. Lett.* **2010**, *35*, 2451.

[14] S. J. Chen, X. Y. Zhao, Y. R. Wang, J. W. Shi, D. H. Liu, *Appl. Phys. Lett.* **2012**, *101*, 123508.

[15] W. Zhou, M. Dridi, J. Y. Suh, C. H. Kim, D. T. Co, M. R. Wasielewski, G. C. Schatz, T. W. Odom, *Nat. Nanotechnol.* **2013**, *8*, 506.

[16] a) D. Wang, A. Yang, W. Wang, Y. Hua, R. D. Schaller, G. C. Schatz, T. W. Odom, *Nat. Nanotechnol.* **2017**, *12*, 889; b) A. K. Yang, T. B. Hoang, M. Dridi, C. Deeb, M. H. Mikkelsen, G. C. Schatz, T. W. Odom, *Nat. Commun.* **2015**, *6*, 6939; c) T. K. Hakala, H. T. Rekola, A. I. Vakevainen, J. P. Martikainen, M. Necada, A. J. Moilanen, P. Torma, *Nat. Commun.* **2017**, *8*, 13687; d) D. Q. Wang, J. Guan, J. T. Hu, M. R. Bourgeois, T. W. Odom, *Acc. Chem. Res.* **2019**, *52*, 2997.

[17] a) W. J. Wang, M. Ramezani, A. I. Vakevainen, P. Torma, J. G. Rivas, T. W. Odom, *Mater. Today* **2018**, *21*, 303; b) R. Li, M. R. Bourgeois, C. Cherqui, J. Guan, D. Wang, J. Hu, R. D. Schaller, G. C. Schatz, T. W. Odom, *Nano Lett.* **2019**, *19*, 6435; c) D. Q. Wang, A. K. Yang, A. J. Hryn, G. C. Schatz, T. W. Odom, *ACS Photonics* **2015**, *2*, 1789; d) R. Guo, T. K. Hakala, P. Torma, *Phys. Rev. B* **2017**, *95*, 155423.

[18] D. Wang, M. R. Bourgeois, W. K. Lee, R. Li, D. Trivedi, M. P. Knudson, W. Wang, G. C. Schatz, T. W. Odom, *Nano Lett.* **2018**, *18*, 4549.

[19] M. P. Knudson, R. Li, D. Q. Wang, W. J. Wang, R. D. Schaller, T. W. Odom, *ACS Nano* **2019**, *13*, 7435.

[20] S. Pourjamal, T. K. Hakala, M. Necada, F. Freire-Fernandez, M. Kataja, H. Rekola, J. P. Martikainen, P. Torma, S. van Dijken, *ACS Nano* **2019**, *13*, 5686.

[21] J. Guan, M. R. Bourgeois, R. Li, J. Hu, R. D. Schaller, G. C. Schatz, T. W. Odom, *ACS Nano* **2021**, *15*, 5567.

[22] Y. Saito, N. Nakai, A. Nomura, T. Kano, *Appl. Opt.* **1992**, *31*, 4298.

[23] M. H. Lee, M. D. Huntington, W. Zhou, J.-c. Yang, T. W. Odom, *Nano Lett.* **2011**, *11*, 311.

[24] a) J. Henzie, E. S. Kwak, T. W. Odom, *Nano Lett.* **2005**, *5*, 1199; b) H. Gao, J. Henzie, T. W. Odom, *Nano Lett.* **2006**, *6*, 2104.

[25] F. P. Schäfer, *Dye Lasers*, Vol. 1, Springer Science & Business Media, Berlin, Germany **2013**.

[26] C. Cie, *International Commission on Illumination*, Cambridge University, Cambridge, UK **1932**.

[27] J. Schanda, *Colorimetry: Understanding the CIE System*, John Wiley & Sons, Hoboken, NJ, USA **2007**.

[28] W. J. Wang, N. Watkins, A. K. Yang, R. D. Schaller, G. C. Schatz, T. W. Odom, *J. Phys. Chem. Lett.* **2019**, *10*, 3301.